Article

Cell Reports

Quantitative Dissection and Modeling of the NF-κB p100-p105 Module Reveals Interdependent Precursor Proteolysis

Graphical Abstract

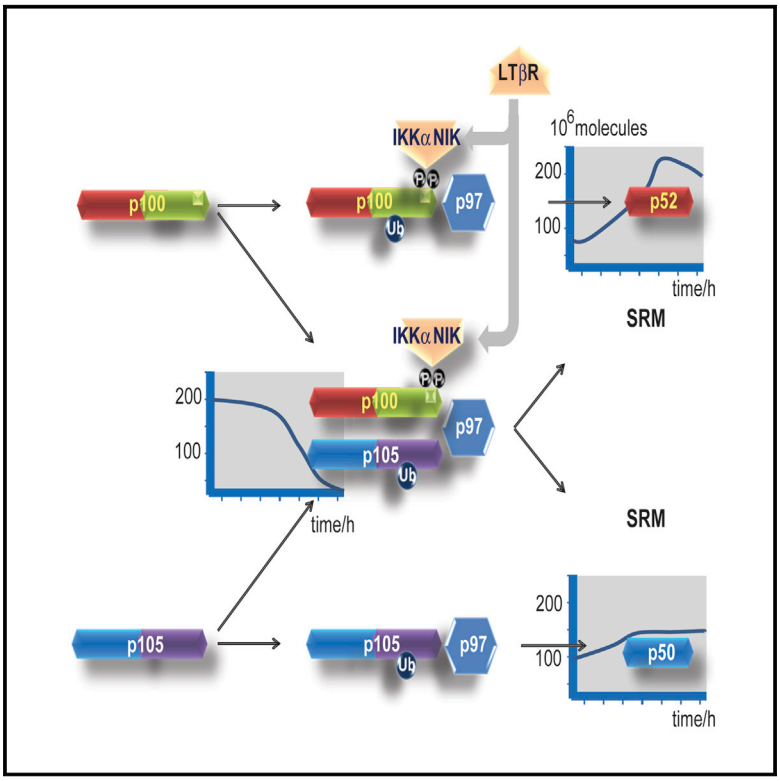

Highlights

LTβR pathway triggers interdependent proteolysis of NF-κB precursors p100 and p105

NIK and IKKα regulate p105 proteolysis through C-terminal degron serines in p100

Cogeneration of p50 and p52 depends on functional VCP/p97

Quantitative mathematical models predict direct signal responsiveness of p100-p105

Authors

Zekiye Buket Yılmaz, Bente Kofahl, ..., Gunnar Dittmar, Claus Scheidereit

Correspondence

yilmaz@mdc-berlin.de (Z.B.Y.),
scheidereit@mdc-berlin.de (C.S.)

In Brief

Proteolytic precursor processing is a hallmark of the NF-κB system. Yilmaz et al. show that in lymphotoxin-stimulated cells p100 acts upstream of p105, resulting in concurrent production of p52 and p50. Both precursors form complexes and bind to segregase (p97/VCP), which promotes proteasomal processing. The findings are supported by mass spectrometry and incorporated in quantitative mathematical models.

Yılmaz et al., 2014, Cell Reports 9, 1756–1769
December 11, 2014 ©2014 The Authors
http://dx.doi.org/10.1016/j.celrep.2014.11.014

OPEN ACCESS
CellPress

Cell Reports
Article

Quantitative Dissection and Modeling of the NF-κB p100-p105 Module Reveals Interdependent Precursor Proteolysis

Zekiye Buket Yılmaz,[1,*] Bente Kofahl,[2] Patrick Beaudette,[1,3] Katharina Baum,[2] Inbal Ipenberg,[1] Falk Weih,[4,5] Jana Wolf,[2,6] Gunnar Dittmar,[3,6] and Claus Scheidereit[1,6,*]

[1]Signal Transduction Laboratory, Max Delbrück Center for Molecular Medicine, Robert-Rössle-Strasse 10, 13125 Berlin, Germany
[2]Mathematical Modeling Group, Max Delbrück Center for Molecular Medicine, Robert-Rössle-Strasse 10, 13125 Berlin, Germany
[3]Mass Spectrometry Group, Max Delbrück Center for Molecular Medicine, Robert-Rössle-Strasse 10, 13125 Berlin, Germany
[4]Leibniz-Institute for Age Research-Fritz-Lipmann-Institute, Beutenbergstrasse 11, 07745 Jena, Germany
[5]Deceased
[6]Co-senior author
*Correspondence: yilmaz@mdc-berlin.de (Z.B.Y.), scheidereit@mdc-berlin.de (C.S.)
http://dx.doi.org/10.1016/j.celrep.2014.11.014

SUMMARY

The mechanisms that govern proteolytic maturation or complete destruction of the precursor proteins p100 and p105 are fundamental to homeostasis and activation of NF-κB; however, they remain poorly understood. Using mass-spectrometry-based quantitative analysis of noncanonical LTβR-induced signaling, we demonstrate that stimulation induces simultaneous processing of both p100 and p105. The precursors not only form hetero-oligomers but also interact with the ATPase VCP/p97, and their induced proteolysis strictly depends on the signal response domain (SRD) of p100, suggesting that the SRD-targeting proteolytic machinery acts in *cis* and in *trans*. Separation of cellular pools by isotope labeling revealed synchronous dynamics of p105 and p100 proteolysis. The generation of p50 and p52 from their precursors depends on functional VCP/p97. We have developed quantitative mathematical models that describe the dynamics of the system and predict that p100-p105 complexes are signal responsive.

INTRODUCTION

The nuclear factor-κB (NF-κB) family of transcription factors comprises p105/p50 (NF-κB1), p100/p52 (NF-κB2), RelA (p65), c-Rel, and RelB and regulates numerous physiological processes by controlling inducible gene expression programs. In resting cells, NF-κB homo- and heterodimers are sequestered in the cytoplasm through their interaction with IκB proteins or with p105 and p100. Although they also are IκBs, p105 and p100 primarily function as precursors for the mature NF-κB proteins p50 and p52, respectively, which are generated by ubiquitin-dependent proteasomal processing (Sun, 2012; Vallabhapurapu and Karin, 2009).

Various stimuli trigger rapid and transient activation of canonical NF-κB pathways resulting in phosphorylation of IκBs through the IκB kinase (IKK) complex that contains the catalytic subunits IKKα and IKKβ and the regulatory subunit IKKγ/NEMO, and in their subsequent proteasomal degradation. In contrast, a subset of tumor necrosis factor receptor (TNFR) family members, such as lymphotoxin beta receptor (LTβR), CD40, B cell activating factor receptor (BAFF-R), or receptor activator of NF-κB (RANK) activate the noncanonical NF-κB pathway, which specifically induces processing of p100 to generate p52 (Hayden and Ghosh, 2008; Razani et al., 2011; Scheidereit, 2006). Noncanonical signaling critically depends on IKKα and NF-κB-inducing kinase (NIK). NIK phosphorylates the T loop serines of IKKα, which then phosphorylates p100 at C-terminal serines, to trigger ubiquitination and proteasomal processing of p100 (Senftleben et al., 2001; Xiao et al., 2001).

Constitutive p105 processing to p50 and complete degradation are the two proteolytic processes that regulate cellular levels of p105 and p50. Stimuli such as lipopolysaccharide, TNF-α, or interleukin (IL)-1α trigger IKKβ-mediated phosphorylation of serines 927 and 932 in a degron sequence of p105 followed by $SCF^{\beta-TrCP}$-mediated ubiquitination. This predominantly promotes proteasomal p105 degradation, although IKKβ-triggered processing of p105 was also proposed (Heissmeyer et al., 1999, 2001; Orian et al., 2000). These observations were largely based on overexpression studies, and evidence of signal-induced p105 processing in physiological settings has not been demonstrated.

Thus far, the regulation of p100 and p105 proteolysis has been considered as independent events. We report here that activation of noncanonical NF-κB signaling by LTβR also results in induced p105 processing and the generation of p50, a process that does not require the reported p105 phospho-acceptor sites but instead is tightly coupled to p100 as the main signal receiving component.

The regulatory mechanisms that control complete versus partial proteolysis of the NF-κB precursor proteins have largely remained elusive. To gain mechanistic insight into the

coregulation of p100 and p105, it is important to dissect stimulus-dependent and -independent processing and degradation events and to study the role of de novo protein synthesis. Hitherto the investigation of the mechanisms of precursor proteolysis was limited to classical pulse-chase and western blot techniques. We have now established dynamic stable isotope-labeled amino acids in cell culture (SILAC) -coupled selected reaction monitoring (SRM) mass spectrometry to quantitatively determine the concentrations of endogenous p105, p100, p50, and p52 over time in LTβR-stimulated mouse embryonic fibroblasts (MEFs) as a model system. SILAC provides an excellent in vivo strategy to label proteins with different stable isotope-containing amino acids and to monitor quantitative differences at the protein level. The targeted SRM approach relies on the quantification of quantotypic peptides that represent the proteins of interest (Holman et al., 2012). SRM has recently been applied to quantify the components of signal transduction pathways such as EGF signaling in mammary epithelial cells (Wolf-Yadlin et al., 2007), and to absolute quantification of proteins in *S. cerevisiae* (Costenoble et al., 2011; Picotti et al., 2009).

SRM is a powerful asset in mathematical modeling of signaling pathways, because precise copy numbers of proteins can be determined at the basal level as well as in a time-resolved manner following cellular stimulation. Thus, we combined SRM-based quantitative data with mathematical modeling to dissect the mechanism underlying the concerted proteolytic responses of p100 and p105 to LTβR activation and present a model that describes an interdependent regulatory network formed by both precursors. Although earlier mathematical models of NF-κB signaling described the dynamics of canonical pathway activation (Basak et al., 2012; Cheong et al., 2008) and an IκB function of p100 (Basak and Hoffmann, 2008; Basak et al., 2007; Shih et al., 2012), the model presented here dissects the processing of p100 and p105.

A fundamental problem still to be solved is how partial proteasomal proteolysis of the NF-κB precursors can be achieved. It has recently been shown that *Drosophila* Ter94 and its mammalian counterpart Valosin-containing protein (VCP)/p97 regulate the partial proteolysis of the transcription factors Ci and Gli3, respectively, to modulate Hedgehog signaling (Zhang et al., 2013). VCP/p97 is a hexameric AAA (ATPases associated with diverse cellular activities) ATPase and chaperone that functions in the modulation of substrate ubiquitination via its interactions with ubiquitin ligases and deubiquitinating enzymes and in various protein degradation pathways by transferring ubiquitinated substrates to the proteasome (Haines, 2010; Meyer et al., 2012). We demonstrate that p97 binds to both p100 and p105 and that its ATPase activity is required for LTβR-triggered processing of p100 and p105.

Collectively, this work provides quantitative and mechanistic insight into noncanonical LTβR signaling and highlights a network that integrates p100 and p105, which may have important implications for the regulation of target genes and for the physiological and pathological functions of precursor-derived NF-κB subunits.

RESULTS AND DISCUSSION

LTβR Induces Simultaneous Proteolysis of p105 and p100 and Generation of p50 and p52

LTβR signaling is a prototype pathway that triggers noncanonical NF-κB activation, in particular, the proteolytic conversion of p100 to p52. We noticed an unexpected and strikingly similar signal responsiveness of p105/p50 and p100/p52. The amount of both precursors significantly declined in the cytoplasm within the first 4 hr (Figure 1A, left), whereas nuclear translocation of p50 and p52, along with RelB, was evident 3 hr poststimulation (Figure 1, right). To allow a faithful, quantitative investigation of precursor proteolysis, a SRM-based technique was established, utilizing N- and C-terminal p100- and p105-specific proteotypic peptides for absolute quantification of precursors and products (Figure 1B; see legend and Table S1 for details). SRM-based mass spectrometry allows quantitation when isotopically heavy analogs of the targeted proteotypic peptides are spiked in during sample preparation at a known concentration.

SRM analysis revealed a stimulus-dependent decrease with similar kinetics for both p105 and p100 and for generation of p50 and p52 (Figure 1B). The increase of p52 was slightly more pronounced than that of p50 (see Figure S1C for nanomolar ranges). Immunoblotting of cytoplasmic extracts did not reveal this increase due to predominant nuclear translocation of the products (Figure 1A, left and right). Nuclear translocation of p50 and p52 was also quantified by SRM analysis of nuclear extracts (Figure S1D), indicating a similar nuclear enrichment.

Signal-induced p100 processing strictly depends on de novo protein synthesis (Claudio et al., 2002; Coope et al., 2002; Mordmüller et al., 2003). Cycloheximide treatment blocks the upregulation of NIK and subsequent p100 processing in BAFF and CD40L-stimulated B cells (Qing et al., 2005). In line with this, LTβR-induced p105 proteolysis and p50 nuclear translocation were also completely impaired in cells treated with cycloheximide (Figure S1E). As seen in MEF, LTβR activation of macrophage and bone marrow stromal cell lines resulted in p105 proteolysis and nuclear accumulation of p50 and p50 DNA binding (Figures S1F and S1G; data not shown), indicating that the responsiveness of p105 to noncanonical signaling is not cell type restricted.

Requirement of NIK, IKKα, and p100 for LTβR-Induced p105 Proteolysis

Extensive studies with a variety of noncanonical NF-κB pathway activating stimuli (BAFF, CD-40, LTβR) in different cell systems established a central role of NIK and IKKα in regulating p100 processing and p52 generation (Claudio et al., 2002; Coope et al., 2002; Dejardin et al., 2002; Senftleben et al., 2001; Xiao et al., 2001; Yilmaz et al., 2003). NIK and IKKα are also essential for LTβR-induced p105 processing to generate p50. LTβR-induced p105 proteolysis was completely abrogated in $nik^{-/-}$, *aly/aly*, or $Ikk\alpha^{-/-}$ MEF and, as a control, in $lt\beta r^{-/-}$ cells, whereas IKKβ and IKKγ/NEMO were dispensable (Figure 2A). The alymphoplasia (*aly*) mutation of the *nik* gene causes a deficiency of NIK in IKKα and TRAF interaction (Luftig et al., 2001; Shinkura et al., 1999). Altogether, the selective requirement of NIK, IKKα, and

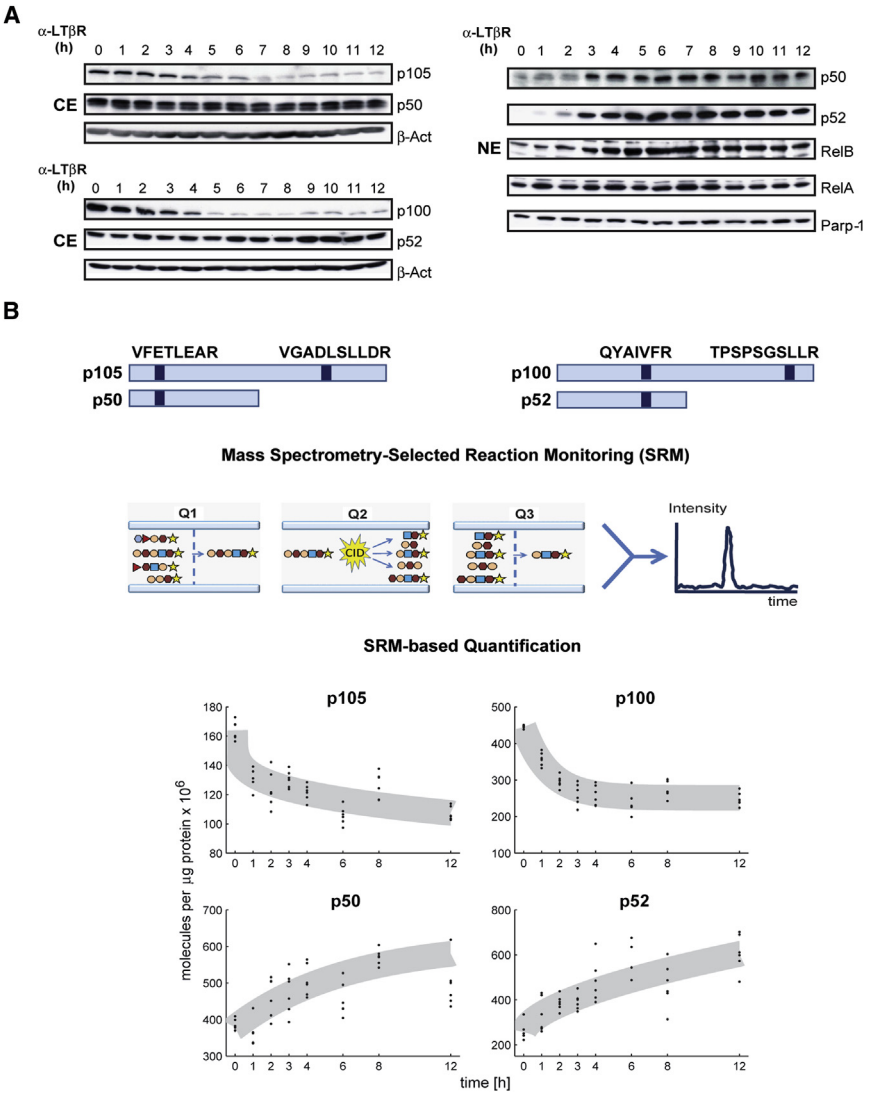

Figure 1. Quantitative Mass-Spectrometry-Based Analysis of LTβR-Induced p105 Proteolysis

(A) Wild-type MEF were stimulated with anti-LTβR agonistic antibody (AC.H6) for 12 hr. Cytoplasmic extracts (CEs) were immunoblotted with p50/p105 or p52/p100 antibodies (left). One of three independent experiments is shown. Nuclear extracts (NE) were analyzed by western blotting (right).

(B) Top, schematic outline of p50/p105- and p52/p100-specific proteotypic peptides and of SRM mass spectrometry. Sequential mass filtering is performed through quadrupoles (Q1–Q3). The peptide of interest is isolated in Q1, followed by collision-induced dissociation (CID) in Q2. Finally, the selected fragment is isolated in Q3, resulting in a measurable ion current.

Bottom, mass-spectrometric quantification of p105, p100, p50, and p52. Wild-type MEF were stimulated with anti-LTβR agonistic antibody (5G11b), and samples at indicated time points were subjected to SRM analysis with C-terminal peptides for p105 and p100, and N-terminal peptides for p50/p105 and p52/p100 (top, dark-blue boxes). For each peptide, three transitions were measured in triplicate injections, with the best two used for quantification according to the highest intensity or absence of coeluting interference. The number of molecules (in millions) per microgram of protein injected was plotted for each of the six quantified measurements (dots). Trend curves are the best fits obtained by performing a least-square fit to a parameterized exponential, logarithmic, or hyperbolic function curve for each species separately, assuming an additive error and normalizing by the SD in each time point. Note that p50 and p52 were quantified by determining the absolute values relative to the heavy standard for the C-terminal p105 and p100 peptides and subtracting these from the absolute values detected for the N-terminal peptides. See Table S1 for peptide positions and transitions. See also Figure S1A for western blots performed with whole-cell extracts (WCEs) prepared from this experiment.

de novo protein synthesis establishes p105 proteolysis and p50 production as part of noncanonical NF-κB signaling downstream of LTβR.

The similarity in the kinetics of p100 and p105 proteolysis, which was also observed in other cell types (data not shown), and the prior characterization of a NIK/IKKα-responsive substrate site only in p100 suggest a coupled process. This prompted us to investigate the reciprocal functional dependencies of the precursors. The requirement of p100 was tested using *p100*$^{-/-}$ cells that are deficient in full-length p100 but were engineered to constitutively express p52 (Ishikawa et al., 1997), and in *nfkb2*$^{-/-}$ cells, lacking both p100 and p52. Strikingly, LTβR-induced p105 proteolysis was completely abrogated in *p100*$^{-/-}$ and *nfkb2*$^{-/-}$ MEF, demonstrating that it strictly depended on p100. The loss of p105 responsiveness was also observed after small interfering RNA (siRNA)-mediated downregulation of p100 (Figure 2B). These results were confirmed by SRM analysis with absolute quantification of p105 in wild-type, *p100*$^{-/-}$, and *nfkb2*$^{-/-}$ MEF. Although LTβR triggered a reduction in p105 concentration of almost 50% in wild-type cells 6 hr poststimulation, p105 concentrations did not change in p100-deficient cells (Figure 2C). Impaired p105 proteolysis in these cells correlated with the lack of nuclear translocation of p50 (Figure S2A, top). Importantly, reconstitution of *p100*$^{-/-}$ MEF with p100 fully restored LTβR-triggered p105 proteolysis, demonstrating that, in addition to NIK and IKKα, p100 acts upstream of p105 proteolysis (Figure 2D). Both precursors are known to interact with their processing products and other NF-κB subunits. However, LTβR-mediated p105 proteolysis did not require RelA or RelB (Figure S2B).

The lack of p105 processing in p100-deficient cells cannot be explained by a loss of function of the upstream components. Albeit reduced in p100-deficient cells, NIK was stabilized upon proteasomal inhibition (Figure S2C). LTβR-mediated TRAF2

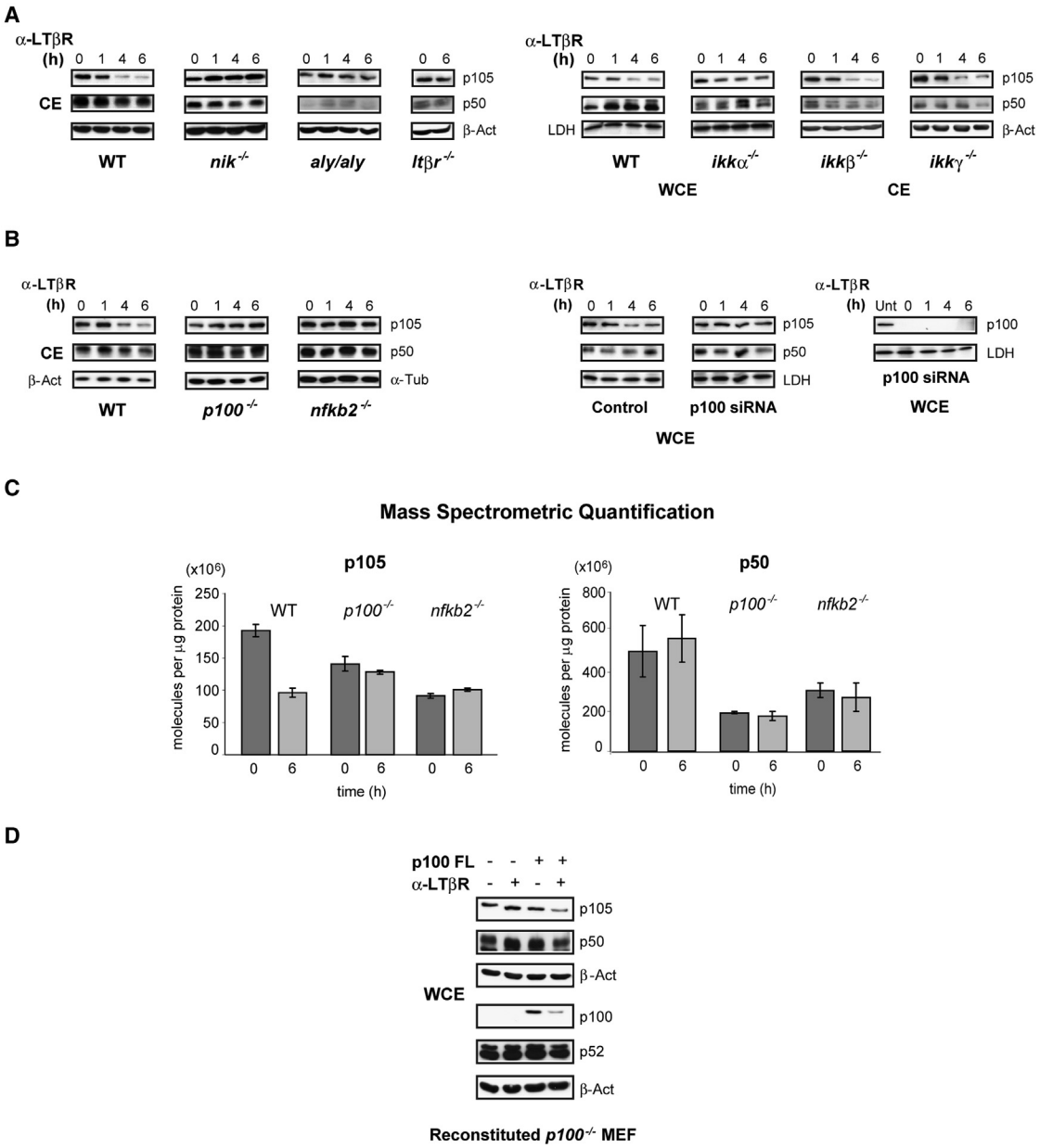

Figure 2. LTβR Induces p105 Proteolysis in a NIK, IKKα, and p100-Dependent Manner

(A) Wild-type, *nik*$^{-/-}$, *aly/aly*, or *ltβr*$^{-/-}$ MEF (left) and *ikkα*$^{-/-}$, *ikkβ*$^{-/-}$, or *ikkγ*$^{-/-}$ MEF (right) were stimulated with 5G11b. CEs or WCEs were immunoblotted with p105 and p50 antibodies. LDH and β-actin were used as loading controls.

(B) Wild-type, *p100*$^{-/-}$, and *nfkb2*$^{-/-}$ MEF were stimulated with 5G11b. Cytoplasmic extracts were immunoblotted with p105 and p50 antibodies (left). Wild-type MEF were transfected with siRNA against p100 or control. On the third day, cells were stimulated with anti-LTβR agonistic antibody (AC.H6) for the indicated time points. WCEs were immunoblotted with p105, p50 (middle), or p100 antibodies (right). Unt, untransfected control.

(C) Wild-type, *p100*$^{-/-}$, and *nfkb2*$^{-/-}$ MEF were left untreated or stimulated with 5G11b for 6 hr. Total p105 (left) and p50 (right) were quantified by SRM as described in Figure 1B. The average of six transitions was plotted as the number of molecules (in millions) per microgram of protein injected. The SDs of these six values are shown by error bars.

(D) *p100*$^{-/-}$ MEF were either mock transfected or transfected with full-length mouse p100 (FL) DNA construct. Twenty-four hours posttransfection, cells were left untreated or stimulated with 5G11b (0.5 μg/ml) for 9 hr. WCEs were immunoblotted with p52/p100, p105, and p50 antibodies.

See also Figure S2.

and TRAF3 degradation were also intact in p100-deficient cells (data not shown). Basal protein levels of the NF-κB members TRAF2, TRAF3, and c-IAP1/2 were comparable in wild-type and p100-deficient MEF (Figure S2D). Most importantly, p100 deficiency did not impair LTβR-mediated IKK activation (Figure S2E).

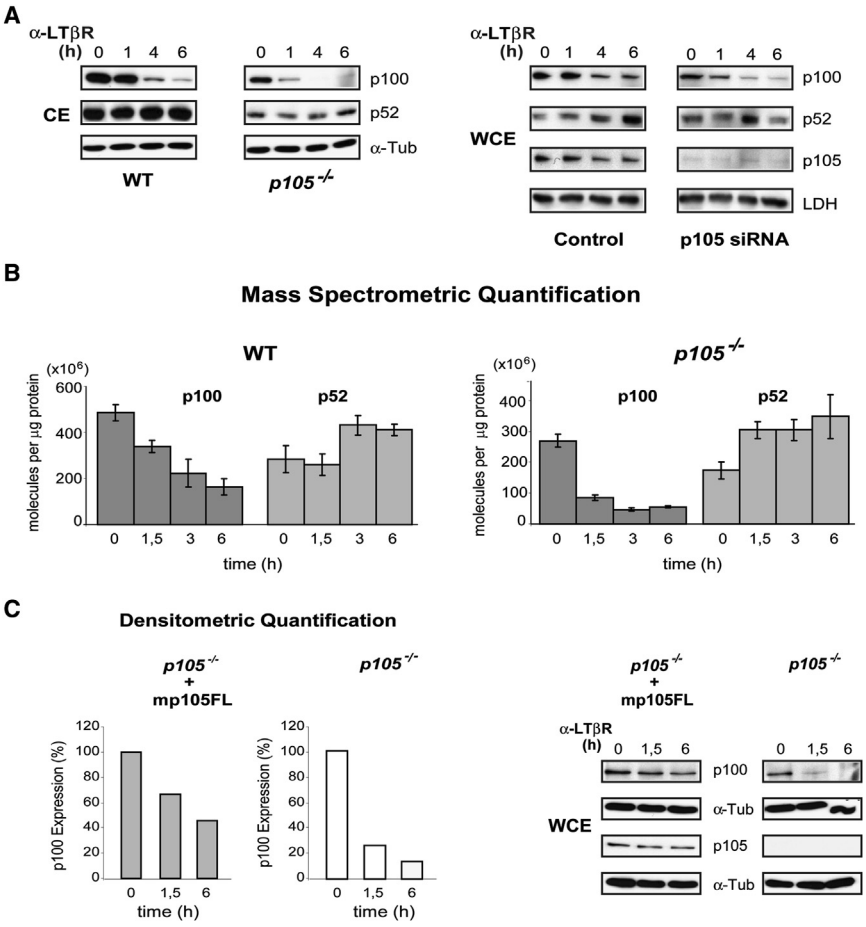

Figure 3. Enhanced LTβR Induced p100 Processing in p105-Deficient Cells

(A) Wild-type and *p105*$^{-/-}$ MEF were stimulated with 5G11b. Cytoplasmic extracts were immunoblotted with p52/p100 antibody (left). WT MEF were transfected with siRNA against p105 or control. The experiment was performed as described in Figure 2B. WCEs were immunoblotted with p52/p100 and p105 antibodies (right).

(B) Wild-type (left) and *p105*$^{-/-}$ MEF (right) were stimulated with 5G11b for the indicated time points. SRM analysis for quantification of p100 and p52 with indicated SD was done as described in Figure 2C.

(C) *p105*$^{-/-}$ MEF were either mock transfected or transfected with full-length mouse p105 (FL) DNA construct. Twenty-four hours posttransfection, cells were left untreated or stimulated with 5G11b (0.5 µg/ml). WCEs were immunoblotted with p100 and p105 antibodies (right). ImageJ software was used for densitometric quantification of p100 band intensities, where signals were normalized against the loading control α-tubulin (left). Unstimulated normalized values were set to 100%.

patches along with the impaired formation of splenic T and B cell zones observed in LTβR-deficient mice was seen in *nfkb1*$^{-/-}$*nfkb2*$^{-/-}$ double mutants, but not in the single knockouts, underlining the significance of a LTβR-p50/p52 signaling axis in vivo (Lo et al., 2006; Remouchamps et al., 2011).

To investigate the functional consequence of the observed reciprocal regulation between p100 and p105, and the simultaneous generation of p50 and p52 (Figures 1, 2, and 3), we analyzed LTβR-responsive genes (Lovas et al., 2008, 2012) by quantitative PCR in *p105*$^{-/-}$, *p100*$^{-/-}$, *nfkb1*$^{-/-}$, and *nfkb2*$^{-/-}$ MEF. A significant fraction of the regulated genes, such as *Vcam-1* and *Traf-1*, required p50 as well as p52 for full induction (Figure S3). These data indicate that p50 and p52 cooperate in the LTβR-activated transcriptional response.

p105 Controls the Efficiency of LTβR-Induced p100 Processing

In contrast to the strict requirement of p100 for induced p105 proteolysis, we found that LTβR-induced p100 processing did not depend on p105. Rather, a strikingly enhanced responsiveness of p100 was observed in LTβR-stimulated *p105*$^{-/-}$ MEF or p105 siRNA-depleted wild-type cells already after 1 hr of stimulation (Figure 3A). SRM analysis further confirmed an almost 3-fold decrease of p100 concentrations in *p105*$^{-/-}$ MEF already 90 min poststimulation, when compared to wild-type cells (Figure 3B). In agreement with enhanced p100 processing, SRM analysis showed an increase of p52 production in stimulated *p105*$^{-/-}$ MEF compared to wild-type cells (Figure 3B). In *p105*$^{-/-}$ MEF reconstituted with full-length p105, the enhanced processing of p100 was reversed to the wild-type situation, demonstrating that p105 has a dampening effect on p100 processing (Figure 3C). Taken together, LTβR-induced proteolyses of p100 and p105 are tightly coupled processes. Although the absence of p100 completely abolishes the LTβR response of p105, the lack of p105 enhances the proteolytic responsiveness of p100.

The contribution of both precursors to noncanonical LTβR signaling is in agreement with the reported knockout phenotypes. The complete absence of lymph nodes and Peyer's

The Destruction Box of p100, but Not p105, Is Required for LTβR-Mediated p105 Proteolysis

Next, we tested if p105 and p100 were able to form heterocomplexes, which may explain the observed interdependent proteolysis. Indeed, gel filtration experiments revealed that in resting or stimulated cells p105 and p100 comigrated in the same high molecular weight (HMW) range (440–669 kDa; Figure 4A). This is in agreement with the previously observed comigration of p100 and p105 in similar HMW fractions (Savinova et al., 2009). Furthermore, both precursors were coimmunoprecipitated in resting or LTβR-activated cells with antibodies against C-terminal epitopes, demonstrating that p105 and p100 heteromerize (Figure 4B). Of note, the migration of p105 from *p100*$^{-/-}$ MEF and of p100 from *p105*$^{-/-}$ MEF were not altered compared to wild-type cells (data not shown), suggesting that the precursors

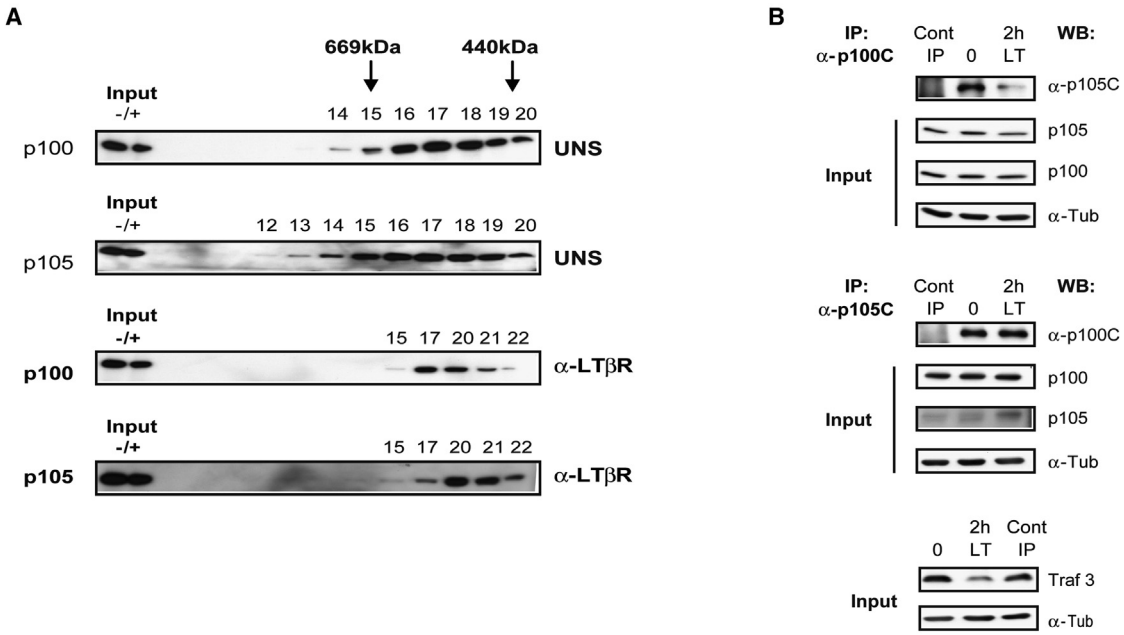

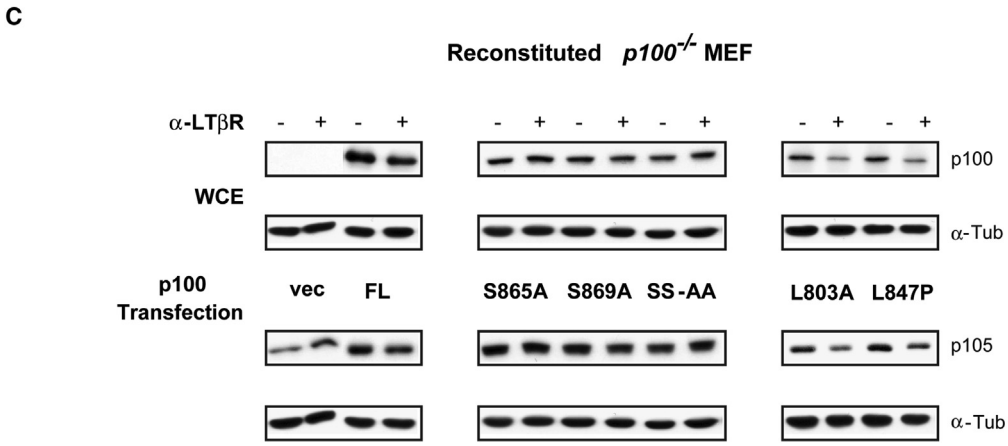

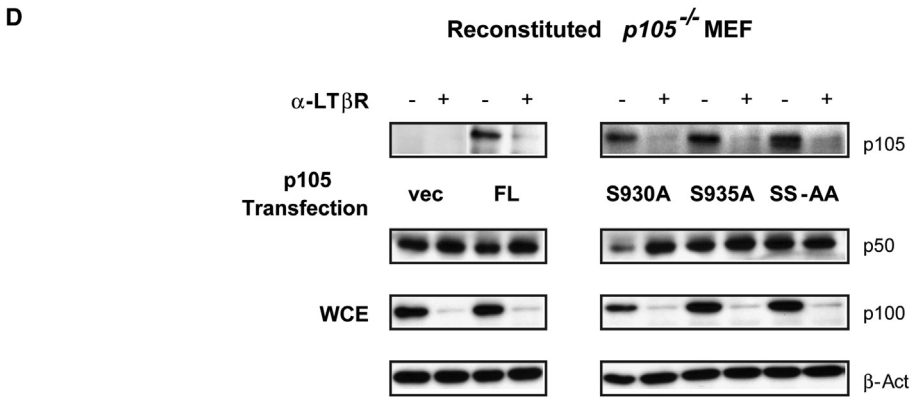

Figure 4. LTβR-Induced p105 Proteolysis Strictly Depends on the C-Terminal Destruction Box of p100

(A) Cytoplasmic extracts of unstimulated and anti-LTβR antibody (5G11b) -stimulated (2 hr) wild-type MEF were fractionated by gel filtration chromatography on an analytical Superose 6 column. Samples from the indicated fractions were analyzed by western blotting to detect p105 and p100. Aliquots of CEs from unstimulated (−) and stimulated (+) cells were taken as input.

(legend continued on next page)

may undergo hetero- as well as homo-oligomerization. As in fibroblasts, endogenous p100-p105 complexes were also observed in RAW264.7 cells and in $CD43^+$ mouse splenic B cells (data not shown).

Signal-induced processing of p100 is mediated by IKKα through phosphorylation at C-terminal serine residues 866 and 870 (Xiao et al., 2001). We addressed the role of the phosphoacceptor sites of p100 for p105 proteolysis by reconstituting $p100^{-/-}$ MEF with the corresponding mutant mouse p100 (mp100, serines 865, and 869 to alanines, respectively). As expected, mp100 SS865/869AA was not polyubiquitinated when coexpressed with NIK in HEK293 cells (data not shown), and LTβR-mediated p100 proteolysis was blocked in cells reconstituted with any one of the p100 serine mutants (Figure 4C). Strikingly, endogenous p105 also failed to respond to the stimulus (Figure 4C). This suggests that only a signal-responsive p100 can restore LTβR-activated p105 proteolysis in p100-deficient cells in *trans*. Reconstitution experiments in $nfkb2^{-/-}$ MEF showed similar results (data not shown).

The conserved C-terminal death domain of mp105 (801–888) and mp100 (764–851) may play a role in critical protein-protein interactions and in precursor oligomerization. It was reported that death domain point mutations in human p100 (L831P) (Fong et al., 2002) and human p105 (L841A) (Beinke et al., 2002) impair p100 processing and TNF-α-mediated p105 proteolysis, respectively. We tested the effect of death domain mutations in mouse p100 (L847P and L803) and observed that these mutations affected neither p100 nor p105 proteolysis (Figure 4C). Importantly, all the serine and death domain point mutant forms of mp100 were still able to interact with endogenous p105, as shown by coimmunoprecipitation data (data not shown). In human p105, serines 927 and 932 are essential for IKKβ-mediated phosphorylation, followed by the recruitment of β-TrCP for signal-induced complete degradation (Heissmeyer et al., 2001). However, the equivalent substrate serine residues in mp105 (serines 930 and 935) were not required for proteolysis of p105 in noncanonical LTβR-dependent signaling (Figure 4D).

Because p105 and p100 form heterocomplexes, the ubiquitin ligases and/or other regulators recruited by the phosphorylated C-terminal degron of p100 may act not only in *cis* on p100, but also in *trans* on p105. The dependence of LTβR-induced p105 proteolysis on the p100 degron may restrict p105 "coprocessing" to noncanonical stimuli that specifically act on the NIK and IKKα-selective p100 degron. In contrast, the p105 degron that triggers complete degradation of p105 has been shown to be essential for canonical signaling, such as optimal TCR-induced NF-κB activation in $CD4^+$ T cells and mature T cell function in vivo (Sriskantharajah et al., 2009) and is not responsive to NIK and IKKα.

p97 Is Recruited to Both p100 and p105 and Regulates Noncanonical NF-κB Activation

The *Drosophila* Ter94 ATPase and the mammalian homolog p97 interact with their substrates, Ci and IκBα, respectively, and thereby regulate their proteolysis (Li et al., 2014; Zhang et al., 2013). To analyze a potential involvement of p97 in p100 and p105 processing, we first tested its interaction with the individual precursors. Indeed, endogenous p97 was associated with both p100 and p105 in resting and stimulated cells (Figure 5A). Coimmunoprecipitation experiments with $p100^{-/-}$ and $p105^{-/-}$ MEF showed that p97 can interact with each precursor independently (data not shown).

To demonstrate that p97 acts at the level of the precursors, we first used, as the simplest established system, ectopic NIK expression, which induces p100 processing in the absence of any additional upstream stimulatory signaling (Qing et al., 2005; Xiao et al., 2001). Either wild-type p97 or a dominant-negative p97 mutant (M39) were cotransfected with NIK. The mutant p97 (M39) is defective in its ATPase function and assembles with endogenous p97 into heteromeric, dysfunctional hexamers. This mutant bears point mutations in the D1 (K251A) and D2 (K524A) ATPase domains (Figure 5B) and effectively inhibits p97 function in the endoplasmic reticulum associated degradation (ERAD) pathway (DeLaBarre et al., 2006). NIK-induced p52 formation was indeed strongly impaired by mutant p97 (M39), but not by wild-type p97 (Figure 5C). The ectopic p97 expression levels were in a similar range compared to endogenous p97 (Figure 5C). The p97 mutation did not affect the interaction with p100, because wild-type and mutant p97 bound to the precursor comparably (Figure 5D). Of note, NIK-induced C-terminal phosphorylation of p100 was unaffected (Figure 5C), suggesting that p97 acts downstream of phosphorylation, e.g., at the level of recruitment of the substrate to the proteasome (Figure S6B).

In order to further investigate the functional role of p97, a potent p97 inhibitor (DBeQ) (Chou et al., 2011), which efficiently blocks the ATPase activity of p97, was used. As shown in Figure 5E, NIK-induced processing of p100 to p52 was reduced following DBeQ treatment. The reduction is more moderate than with p97 M39 because NIK-induced p100 processing was ongoing before DBeQ addition. Collectively, these experiments demonstrate that an impairment of functional p97 either through dominant-negative mutant expression or chemical inhibition interferes with NIK-induced p100 processing.

Li et al. reported that p97 depletion blocks IκBα degradation in TNF-α-stimulated cells (Li et al., 2014). Indeed, siRNA-mediated p97 depletion resulted in the impairment of TNF-α-induced activation of canonical NF-κB (Figure 5F). The TNF superfamily member LIGHT predominantly activates noncanonical NF-κB

(B) Unstimulated and stimulated (5G11b) wild-type MEF were lysed after 2 hr, and full-length p105 and p100 precursors were immunoprecipitated with C-terminal antibodies. Coimmunoprecipitation of precursors was detected by western blotting with C terminus-specific antibodies (α-p100C and α-p105C, respectively). As stimulation control, TRAF3 degradation is shown.

(C) $p100^{-/-}$ MEF were either mock transfected (vec) or transfected with full-length mouse p100 (FL), serine point mutants (S865A, S869A, SS865,869AA), or death domain point mutants (L803A, L847P). Twenty-four hours posttransfection, cells were either left untreated or stimulated with 5G11b (0.5 μg/ml) for 24 hr. WCEs were immunoblotted with p100 and p105 antibodies.

(D) $p105^{-/-}$ MEF were either mock transfected or transfected with full-length mouse p105 (FL), or serine point mutants (S930A, S935A, SS930,935AA). WCEs were analyzed as described in (C).

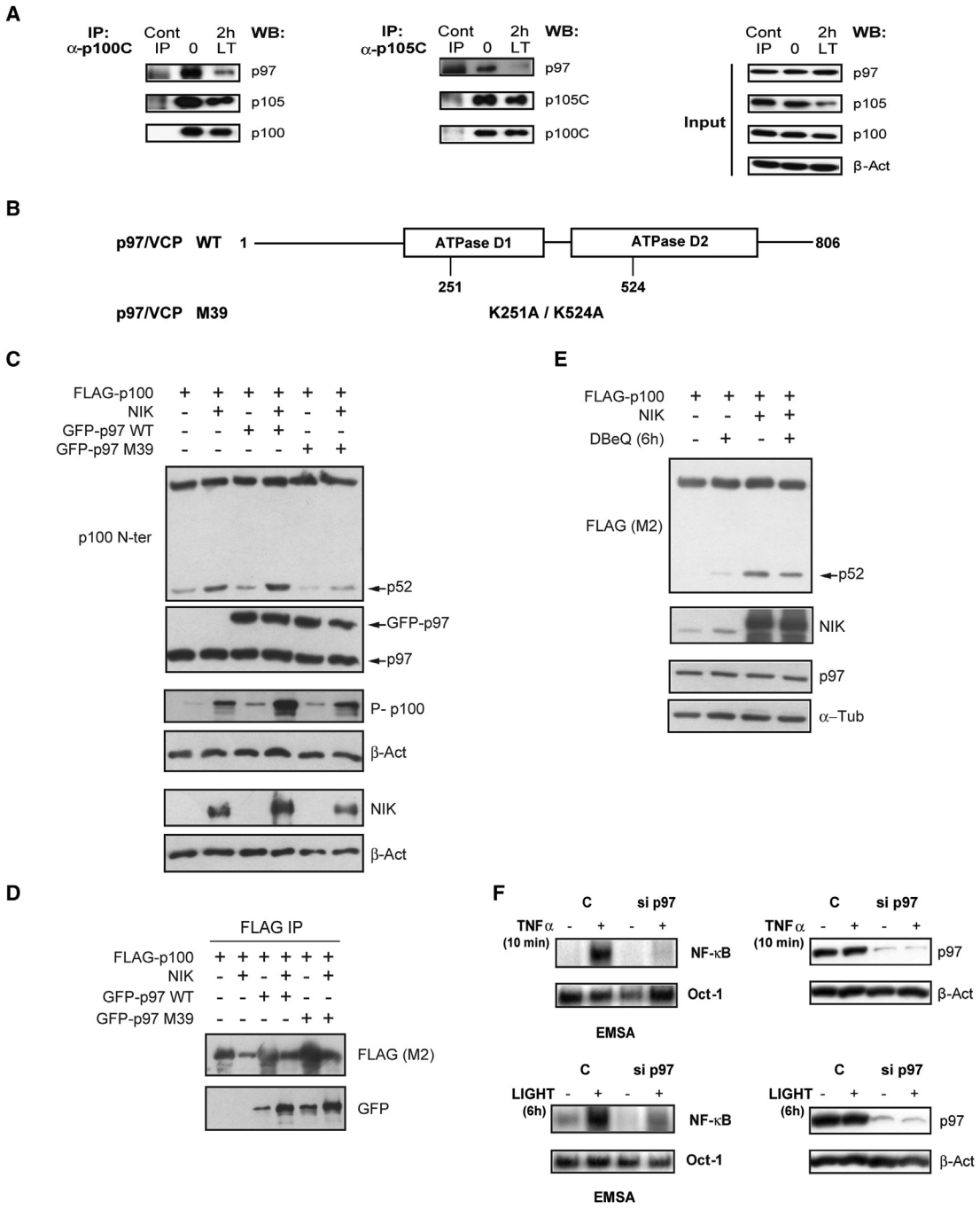

Figure 5. Precursor Processing and Noncanonical NF-κB Activation Is Regulated by p97

(A) Immunoprecipitations of full-length precursors were performed as in Figure 4B. Coimmunoprecipitation of precursors with p97 was detected by western blotting.

(B) Scheme of wild-type human p97 and its dominant-negative (DN) form, M39.

(C) HEK293 cells were transfected with FLAG-p100 construct with or without NIK coexpression and with wild-type GFP-p97 (WT) or p97 DN (M39) expression. Forty-eight hours posttransfection cells were lysed and assayed by immunoblotting. A representative sample of three experiments is shown.

(D) In the experimental setting as described in (C), FLAG-p100 was immunoprecipitated by FLAG M2 resin, and the eluates were analyzed for GFP-p97 interaction by immunoblotting.

(E) HEK293 cells were transfected with FLAG-p100 construct with or without NIK coexpression. Twenty-four hours posttransfection, cells were treated with DMSO or 10 μM DBeQ for 6 hr. NIK-mediated p100 processing was assayed by immunoblotting.

(F) HeLa cells were transfected with siRNAs against p97 or control (C). Seventy-two hours posttransfection, cells were either left untreated or were stimulated with TNF-α (20 ng/ml) for 10 min (top) or with LIGHT (100 ng/ml) for 6 hr (bottom). CEs were immunoblotted for knockdown efficiency (right). NF-κB activation and Oct-1 as loading control were assayed with EMSA (left) as described previously (Stilmann et al., 2009).

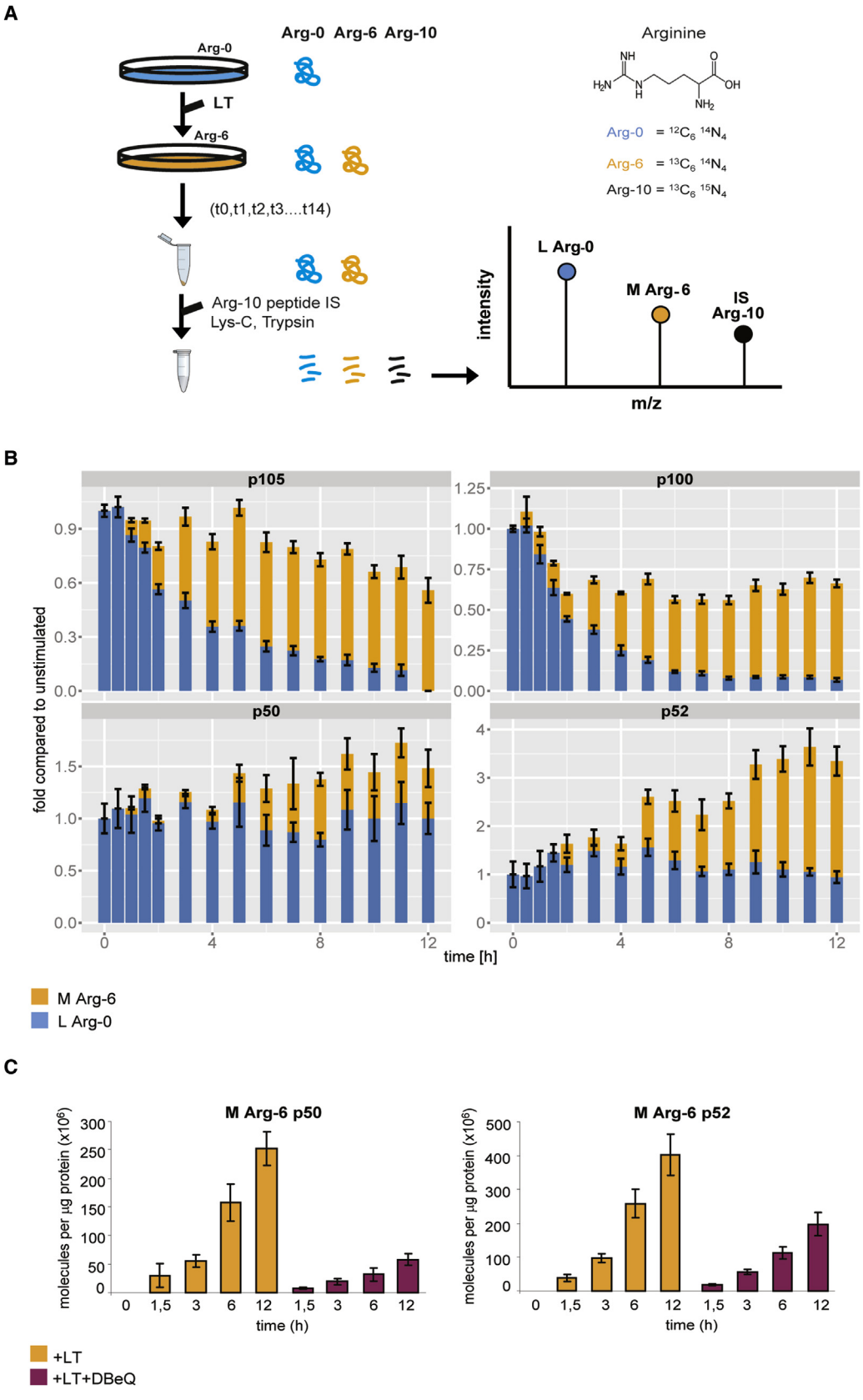

(legend on next page)

(Mordmüller et al., 2003) through LTβR ligation (Kim et al., 2005). Depletion of p97 significantly reduced LIGHT-induced noncanonical NF-κB activity (Figure 5F, bottom left). Whereas Li et al. (2014) demonstrated p97 recruitment to IκBα, we show that p97 is recruited to the NF-κB precursors and that p97 inhibition blocks stimulus-induced NF-κB DNA binding activities in the canonical as well as in the noncanonical pathway.

Dissection of Subpopulations by Dynamic SILAC-SRM Reveals Equivalent LTβR-Induced p50 and p52 Generation that Requires p97 ATPase Activity

The requirement of translation for precursor processing in noncanonical signaling was previously investigated, and cotranslational mechanisms for p50 and p52 generation have been suggested (Heusch et al., 1999; Lin et al., 2000; Mordmüller et al., 2003). However, multiple processes (precursor synthesis, degradation, processing, and turnover of the products) have to be considered. Thus, to further scrutinize the equivalent dynamics of LTβR-stimulated p100 and p105 proteolysis and of the generation of their products, we performed SILAC-SRM experiments. This allows to trace protein populations that were translated before or after adding M Arg-6 isotope labeled medium to cells initially grown in L Arg-0 medium (Figure 6A). SRM analysis of these samples revealed distinct dynamics of the two populations designated as proteins^{L}, containing L Arg-0, and proteins^{M}, containing M Arg-6 (Figure 6B, blue and orange bars, respectively). Relative p105^{L} and p100^{L} levels (blue) decreased over time, leading to an overall loss of almost 90% of both precursors^{L}, whereas relative levels of p50^{L} and p52^{L} did not show a strong alteration. In contrast, the relative levels of precursors^{M} and products^{M} increased over time, such that an overall gain in p50 and p52 was observed in the M population (Figure 6B, orange bars). As expected, the accumulation of p50^{M} and p52^{M} was almost completely abolished by cycloheximide or proteasome inhibitor (MG132) treatment (Figure S5A), whereas p50^{L} and p52^{L} were unaffected (Figure S5B). Thus, the overall dynamics of the two populations of precursors and their products in response to LTβR signaling reveal a striking similarity. The quantitative data obtained by SILAC-SRM served as a basis for mathematical models to dissect the various processes regulating the interdependent reactions of both precursors to LTβR stimulation (see below).

In order to investigate the functional role of p97 in LTβR-induced processing of p100 and p105, the p97 inhibitor DBeQ was used in dynamic SILAC experiments. Of note, DBeQ treatment alone did not show any adverse effects on total protein levels of NIK, TRAF2, or TRAF3 (data not shown). Although DBeQ treatment barely affected p50^{L} and p52^{L} concentrations (Figure S5B), p97 inhibition significantly reduced the accumulation of p50^{M} and p52^{M} (Figure 6C; see also Figure S6A for effects on basal processing and on precursors). Thus, p97 is required for LTβR-induced processing of p100 and p105. Consequently, p97 inhibition similarly affects the dynamics of both products^{M}.

A main function of p97 is the conversion of energy generated through ATP hydrolysis into mechanical force to dissociate protein complexes or extract proteins from intracellular structures such as the ER membrane (Baek et al., 2013; Yamanaka et al., 2012). Hence, one plausible scenario is that the p97 complex may pull out the N-terminal parts of the precursors from the proteasome to rescue them from complete degradation. In the absence of p97 ATPase activity (DBeQ treatment), this rescue mechanism may fail and lead to complete degradation of p105^{M} and p100^{M}, which is in line with the significant decrease in p50^{M} and p52^{M} concentrations. Indeed, DBeQ treatment caused reduced precursor^{M} levels (Figure S6A). That the precursors are reduced proportionally to the diminished formation of their products in presence of DBeQ may indicate that in the absence of p97 function complete precursor degradation may occur, instead of processing. This is the case for basal, as well as for induced processing.

Overall, our data suggest a potential mechanistic explanation how the proteasome may be guided for partial versus complete degradation of NF-κB precursors upon LTβR activation (see also Figure S6B).

Quantitative Modeling Reveals Direct Responsiveness of the p100-p105 Complex to LTβR Activation

Given the intricate interdependency of both precursors, mathematical models were designed to gain insight into the concerted signal responsiveness of p100 and p105 and to investigate the contribution of the p100-p105 complex for the dynamics of the system. We thus developed a set of mathematical models, which describe the different possible fates of the p100-p105 complex (Figure 7A; see the Supplemental Information, development of

Figure 6. Dynamic SILAC-Based Mass Spectrometry Unfolds a Concerted Proteolytic Response of p100 and p105 to LTβR Activation and a Requirement for p97

(A) Schematic presentation of dynamic SILAC experiments. Cells were grown in SILAC light (L Arg-0) medium for several passages. On the day of the experiment, L Arg-0 medium was replaced with SILAC (M Arg-6) medium (t0), with or without LTβR stimulation (LT). Samples were collected, processed for mass spectrometry, and proteins quantified via SRM analysis. The internal standard peptide (IS) is identical in sequence to each of the SRM peptides used in the analysis, except for containing the heavy isotope Arg-10. Note the mass differences in m/z spectra (SRM transitions, see Table S1) resulting from the different arginine isotopes. See also Figure S4.

(B) L Arg-0 medium was exchanged with M-Arg-6 medium containing the agonistic LTβR antibody 5G11b. Wild-type MEF samples were collected at the time points indicated. The unstimulated sample was treated with M-Arg-6 medium only and was collected with the 30 min sample. A representative sample of three experiments is shown, where p105, p50, p100, and p52 were quantified following SRM analysis. Fold changes in the differently labeled proteins relative to the respective unstimulated protein^{L} levels at t = 0 were plotted as stacked bar graphs. The blue bars denote p105^{L}, p50^{L}, p100^{L}, p52^{L} proteins (L Arg-0), whereas the orange bars show p105^{M}, p50^{M}, p100^{M}, p52^{M} proteins (M Arg-6). Note that for this experiment, p105^{L} at 12 hr time point was below detection limit.

(C) Wild-type MEF were subjected to dynamic SILAC with 5G11b antibody, in the absence (orange) or presence (red) of p97 inhibitor DBeQ (N2,N4-dibenzylquinazoline-2,4-diamine). M Arg-6 p50 (p50^{M}) and M Arg-6 p52 (p52^{M}) were quantified following SRM analysis. The average of six transitions was plotted as the number of molecules (in millions) per microgram of protein injected. Error bars represent the SDs of these six values. One of three experiments is shown. See also Figure S6A.

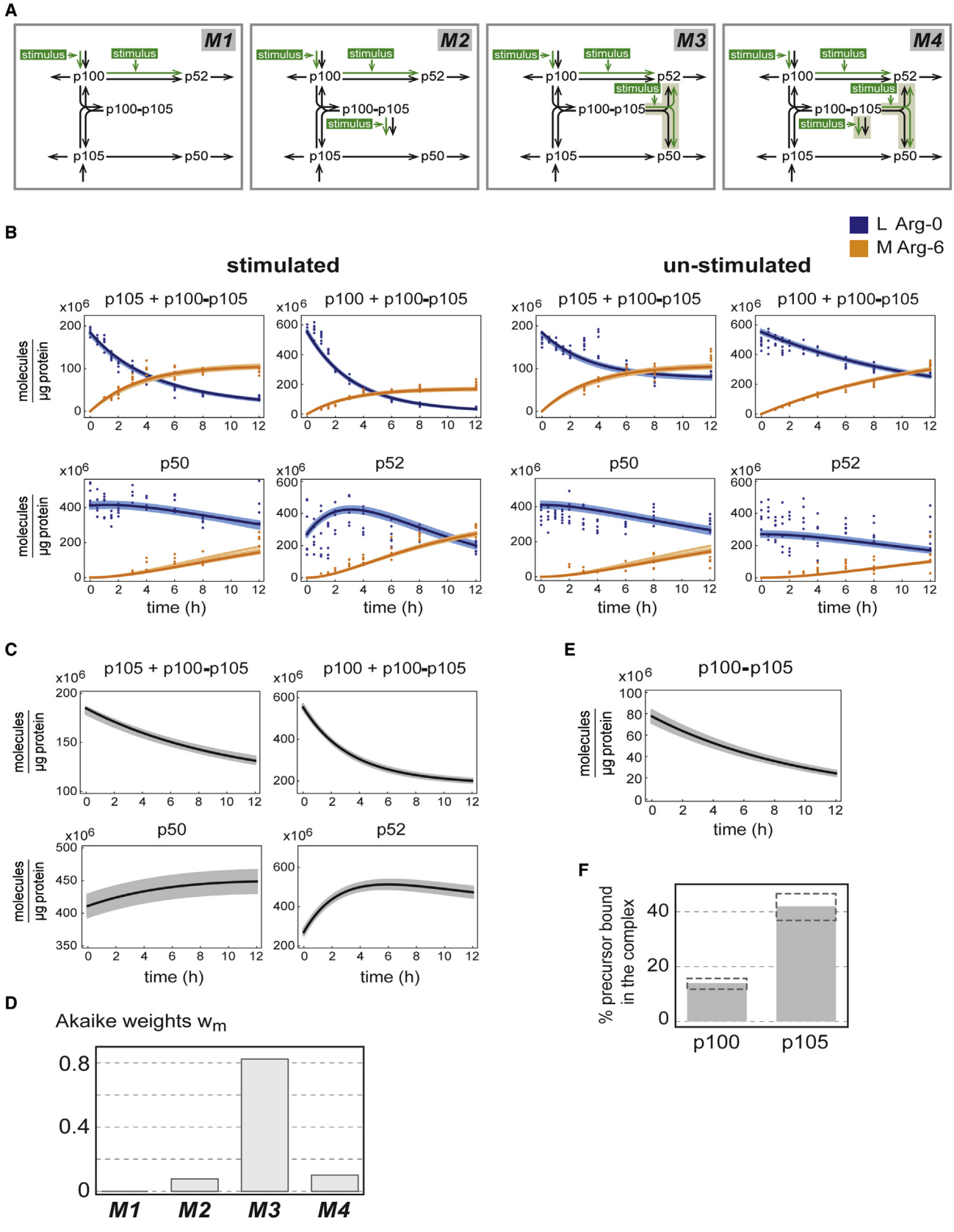

(legend on next page)

the set of mathematical models). The kinetic parameters of the models were estimated by fitting each model to the temporal changes of the absolute numbers of p100, p105, p52, and p50 molecules that were measured by quantitative SILAC-SRM under stimulated and unstimulated conditions. Simulations are shown exemplarily for model M3, using its best-fitting parameters, in comparison with the SILAC-SRM data in Figure 7B (for details of the fitting procedure, see the Supplemental Information, experimental data, model fitting, and parameter estimation, and Table S2). All models were qualitatively in accordance with the SRM and western blot data describing LTβR-induced temporal concentration changes of p100, p105, p52, and p50 (compare Figure 1 with Figure 7C). For further validation, the data obtained for NIK, IKKα, or LTβR mutant cells (Figure 2A), p105-deficient cells (Figure 3), and p97 inhibition (Figures 6C and S6) were qualitatively reproduced by model simulations, as shown in Figures S7B–S7D for model M3. Importantly, these data have not been used for model development and parameter fitting (for details of the validation procedure, see the Supplemental Information, model validation).

The fit quality of the models was compared with Akaike weights (Burnham and Anderson, 2004) (see the Supplemental Information, corrected Akaike information criterion [AIC_c]). The Akaike weights revealed that probability to be the best model is 82% for M3 and 10% and around 8% for M4 and M2, respectively, and negligible ($5*10^{-26\%}$) for M1 (Figure 7D). Hence, M3, in which the p100-p105 complex components undergo signal-induced processing, is the most likely model. Models M2 and M4, in which p100-p105 is subject to inducible degradation or combined inducible processing and degradation, respectively, are considerably less but still likely. In contrast, model M1, which considers p100-p105 as nonresponsive complex, can be rejected due to its low Akaike weight. Similar results have been obtained for extended models that include inducible p100 degradation or allow for different parameters for the species^M and species^L (see Figure S7F).

In addition, the mathematical models allow to predict the concentrations of the p100-p105 complex and to trace its absolute temporal behavior upon LTβR stimulation (Figure 7E for M3). Calculations showed that around 14% of total p100 and around 42% of total p105 are involved in p100-p105 complex formation (Figure 7F). An analysis of models M2 and M4 yielded similar values for their best fits (Table S4).

Taken together, mathematical modeling clearly revealed that the p100-p105 complex is directly signal responsive.

In summary, this work provides a quantitative dissection and modeling of the NF-κB precursor network and reports an unexpected functional hierarchy between p100 and p105 along with the discovery of a p97 requirement for cogeneration of p50 and p52. Importantly, the gain of p50 and p52 from newly synthesized precursors could implicate that de novo synthesized precursors have a particular conformation, state of posttranslational modifications or protein associations, permissive for processing, that is transformed after a yet-unknown time into a state that allows only complete degradation. The experimental definition of these events and the mechanistic details of p97 action will be subject to subsequent studies.

The coupled responsiveness of both precursors to lymphotoxin signaling also explains why only *nfkb1*$^{-/-}$*nfkb2*$^{-/-}$ double knockout shares the complete defect in lymph node formation and splenic microarchitecture observed in LTβR-deficient mice. Taken together, the data presented here provide compelling evidence that demands a profound revision of our understanding of noncanonical NF-κB activation downstream of LTβR.

EXPERIMENTAL PROCEDURES

Cell Culture and Reagents

MEF, HEK293, and HeLa cells were cultured in Dulbecco's modified Eagle's medium (DMEM, GIBCO, for MEF DMEM-Glutamax) supplemented with 10% fetal bovine serum (Gibco; for MEF 10% heat inactivated bovine calf serum HyClone, Thermo Scientific), penicillin (100 U/ml), and streptomycin (100 μg/ml). MEFs were stimulated with the agonistic anti-LTβR antibodies AC.H6 (0.3 μg/ml; BD Pharmingen), 5G11b (0.3 μg/ml) (Daller et al., 2011), and 4H8 WH2 (2 μg/ml; Adipogen) (Dejardin et al., 2002). Specificity was confirmed by using isotype-matched control Ha4/8 (BD Pharmingen) for AC.H6 (Figure S1B), and LTβR-deficient MEF for 5G11b and 4H8 WH2. HeLa cells were stimulated with LIGHT (100 ng/ml; Enzo Life Sciences). Cycloheximide (Calbiochem) was used at 10 μg/ml, and MG132 (Alexis) and DBeQ (BioVision Technologies) were used at 10 μM final concentration.

Figure 7. Mathematical Modeling Underscores Signal Responsiveness of p100-p105 Complexes

(A) Mathematical models including the production, interaction, degradation, and processing of the precursors p100 and p105, as well as the production and degradation of the products p52 and p50. Four different models (M1–M4) were considered which differ in the fate of the p100-p105 complex. In M1, the complex components are neither degraded nor processed, whereas in M2 the precursors in the complex are only degraded in a stimulus-dependent or -independent manner. In M3, stimulus-dependent and -independent exclusive processing of p100 and p105 in the complex are considered. M4 allows for both degradation and processing of the p100-p105 complex. A detailed description of the models is given in the Supplemental Information.

(B) Simulated time courses of model M3 (curves) fitted to the quantitative, time-resolved SILAC data under stimulated and unstimulated conditions (dots) for labeled precursors and products. The results according to the best-fitting parameter set (dark curves) and the 95% confidence intervals of the parameters obtained by parameter profile likelihood estimation (light curves) are given. Measured (simulated) L Arg-0- and M Arg-6-labeled species are represented by blue and orange dots (curves), respectively.

(C) Total p105 (p105 + p100-p105) and total p100 (p100 + p100-p105) were simulated as the sum of stimulated L Arg-0 and M Arg-6 species, according to M3 with parameter sets used for Figure 7B (compare to SRM analysis in Figure 1B).

(D) Akaike weights for models M1 to M4 (differences of the corrected Akaike information criterion (ΔAICc) of the best fit for each model to the minimal AICc, obtained for model M3, are given in Figure S7E).

(E) The simulated (M3) temporal change of the p100-p105 complex concentration in response to LTβR activation is shown.

(F) Fractions of the precursors bound in the p100-p105 complex at unstimulated steady state are given for the best parameter set of M3 (gray bar) and the 95% confidence interval, as estimated by parameter profile likelihood (dotted frame).

See also Figure S7.

Antibodies

RelA/p65 (sc-372), RelB (sc-226), p52/p100 (sc-7386), p50/p105 (sc-1192, sc-8414, sc-114), TRAF2 (sc-876), TRAF3 (sc-947), and c-*jun* (sc-45) antibodies were from Santa Cruz Biotechnology. Anti-p100C, β-Actin, α-Tubulin, and FLAG M2 antibodies were from Sigma-Aldrich. Anti-p105C (4717), IKKα (2682), NIK (4994), and phospho p100 (4810) antibodies were from Cell Signaling. GFP antibody was from Abcam. Anti-cIAP1/2, anti-LDH, and p97 antibodies were from R&D Systems, Chemicon International, and Progen, respectively.

The Supplemental Experimental Procedures can be found in the Supplemental Information section.

SUPPLEMENTAL INFORMATION

Supplemental Information includes Supplemental Experimental Procedures, seven figures, and five tables and can be found with this article online at http://dx.doi.org/10.1016/j.celrep.2014.11.014.

AUTHOR CONTRIBUTIONS

Z.B.Y. performed the biochemical and cell biological experiments. P.B. developed the SRM procedure and performed mass spectrometry (MS) measurements. G.D. conceived and designed the MS analyses. B.K., K.B., and J.W. designed mathematical models. B.K. and K.B. performed model simulations and statistical analyses. I.I. performed biochemical analyses of p97. Z.B.Y. and C.S. wrote the manuscript with feedback of J.W., G.D., and all other authors. F.W. provided advice and material. B.K. and P.B. contributed equally to this work. All authors contributed to the discussion of the results. Along with Z.B.Y., G.D., and J.W., C.S. conceived the study and supervised the project.

ACKNOWLEDGMENTS

We thank Sabine Jungmann and Sandra Rohrmoser for excellent technical assistance. We thank Anup Arumughan for p97 constructs and discussions. We also thank Ruth Schmidt-Ullrich, Marc Riemann, Michael Hinz, Seda Coel Arslan, Felix Oden, Kristina Schradi, Uwe Benary, and Niklas Hartung for valuable discussions and reagents. This work was supported in part by grants from BMBF (ProSiTu) to G.D., J.W., and C.S and from the Helmholtz Association (MSBN Systems Biology) to J.W. and C.S. Our paper is dedicated to the memory of Falk Weih.

Received: February 7, 2014
Revised: October 20, 2014
Accepted: November 8, 2014
Published: December 4, 2014

REFERENCES

Baek, G.H., Cheng, H., Choe, V., Bao, X., Shao, J., Luo, S., and Rao, H. (2013). Cdc48: a swiss army knife of cell biology. J. Amino Acids *2013*, 183421.

Basak, S., and Hoffmann, A. (2008). Crosstalk via the NF-kappaB signaling system. Cytokine Growth Factor Rev. *19*, 187–197.

Basak, S., Kim, H., Kearns, J.D., Tergaonkar, V., O'Dea, E., Werner, S.L., Benedict, C.A., Ware, C.F., Ghosh, G., Verma, I.M., and Hoffmann, A. (2007). A fourth IkappaB protein within the NF-kappaB signaling module. Cell *128*, 369–381.

Basak, S., Behar, M., and Hoffmann, A. (2012). Lessons from mathematically modeling the NF-κB pathway. Immunol. Rev. *246*, 221–238.

Beinke, S., Belich, M.P., and Ley, S.C. (2002). The death domain of NF-kappa B1 p105 is essential for signal-induced p105 proteolysis. J. Biol. Chem. *277*, 24162–24168.

Burnham, K.P., and Anderson, D.R. (2004). Multimodel Inference Understanding AIC and BIC in Model Selection. Sociol. Methods Res. *33*, 261–304.

Cheong, R., Hoffmann, A., and Levchenko, A. (2008). Understanding NF-kappaB signaling via mathematical modeling. Mol. Syst. Biol. *4*, 192.

Chou, T.F., Brown, S.J., Minond, D., Nordin, B.E., Li, K., Jones, A.C., Chase, P., Porubsky, P.R., Stoltz, B.M., Schoenen, F.J., et al. (2011). Reversible inhibitor of p97, DBeQ, impairs both ubiquitin-dependent and autophagic protein clearance pathways. Proc. Natl. Acad. Sci. USA *108*, 4834–4839.

Claudio, E., Brown, K., Park, S., Wang, H., and Siebenlist, U. (2002). BAFF-induced NEMO-independent processing of NF-kappa B2 in maturing B cells. Nat. Immunol. *3*, 958–965.

Coope, H.J., Atkinson, P.G., Huhse, B., Belich, M., Janzen, J., Holman, M.J., Klaus, G.G., Johnston, L.H., and Ley, S.C. (2002). CD40 regulates the processing of NF-kappaB2 p100 to p52. EMBO J. *21*, 5375–5385.

Costenoble, R., Picotti, P., Reiter, L., Stallmach, R., Heinemann, M., Sauer, U., and Aebersold, R. (2011). Comprehensive quantitative analysis of central carbon and amino-acid metabolism in Saccharomyces cerevisiae under multiple conditions by targeted proteomics. Mol. Syst. Biol. *7*, 464.

Daller, B., Müsch, W., Röhrl, J., Tumanov, A.V., Nedospasov, S.A., Männel, D.N., Schneider-Brachert, W., and Hehlgans, T. (2011). Lymphotoxin-β receptor activation by lymphotoxin-α(1)β(2) and LIGHT promotes tumor growth in an NFκB-dependent manner. Int. J. Cancer *128*, 1363–1370.

Dejardin, E., Droin, N.M., Delhase, M., Haas, E., Cao, Y., Makris, C., Li, Z.W., Karin, M., Ware, C.F., and Green, D.R. (2002). The lymphotoxin-beta receptor induces different patterns of gene expression via two NF-kappaB pathways. Immunity *17*, 525–535.

DeLaBarre, B., Christianson, J.C., Kopito, R.R., and Brunger, A.T. (2006). Central pore residues mediate the p97/VCP activity required for ERAD. Mol. Cell *22*, 451–462.

Fong, A., Zhang, M., Neely, J., and Sun, S.C. (2002). S9, a 19 S proteasome subunit interacting with ubiquitinated NF-kappaB2/p100. J. Biol. Chem. *277*, 40697–40702.

Haines, D.S. (2010). p97-containing complexes in proliferation control and cancer: emerging culprits or guilt by association? Genes Cancer *1*, 753–763.

Hayden, M.S., and Ghosh, S. (2008). Shared principles in NF-kappaB signaling. Cell *132*, 344–362.

Heissmeyer, V., Krappmann, D., Wulczyn, F.G., and Scheidereit, C. (1999). NF-kappaB p105 is a target of IkappaB kinases and controls signal induction of Bcl-3-p50 complexes. EMBO J. *18*, 4766–4778.

Heissmeyer, V., Krappmann, D., Hatada, E.N., and Scheidereit, C. (2001). Shared pathways of IkappaB kinase-induced SCF(betaTrCP)-mediated ubiquitination and degradation for the NF-kappaB precursor p105 and IkappaBalpha. Mol. Cell. Biol. *21*, 1024–1035.

Heusch, M., Lin, L., Geleziunas, R., and Greene, W.C. (1999). The generation of nfkb2 p52: mechanism and efficiency. Oncogene *18*, 6201–6208.

Holman, S.W., Sims, P.F., and Eyers, C.E. (2012). The use of selected reaction monitoring in quantitative proteomics. Bioanalysis *4*, 1763–1786.

Ishikawa, H., Carrasco, D., Claudio, E., Ryseck, R.P., and Bravo, R. (1997). Gastric hyperplasia and increased proliferative responses of lymphocytes in mice lacking the COOH-terminal ankyrin domain of NF-kappaB2. J. Exp. Med. *186*, 999–1014.

Kim, Y.S., Nedospasov, S.A., and Liu, Z.G. (2005). TRAF2 plays a key, nonredundant role in LIGHT-lymphotoxin beta receptor signaling. Mol. Cell. Biol. *25*, 2130–2137.

Li, J.M., Wu, H., Zhang, W., Blackburn, M.R., and Jin, J. (2014). The p97-UFD1L-NPL4 protein complex mediates cytokine-induced IκBα proteolysis. Mol. Cell. Biol. *34*, 335–347.

Lin, L., DeMartino, G.N., and Greene, W.C. (2000). Cotranslational dimerization of the Rel homology domain of NF-kappaB1 generates p50-p105 heterodimers and is required for effective p50 production. EMBO J. *19*, 4712–4722.

Lo, J.C., Basak, S., James, E.S., Quiambo, R.S., Kinsella, M.C., Alegre, M.L., Weih, F., Franzoso, G., Hoffmann, A., and Fu, Y.X. (2006). Coordination between NF-kappaB family members p50 and p52 is essential for mediating LTbetaR signals in the development and organization of secondary lymphoid tissues. Blood *107*, 1048–1055.

Lovas, A., Radke, D., Albrecht, D., Yilmaz, Z.B., Möller, U., Habenicht, A.J., and Weih, F. (2008). Differential RelA- and RelB-dependent gene transcription in LTbetaR-stimulated mouse embryonic fibroblasts. BMC Genomics *9*, 606.

Lovas, A., Weidemann, A., Albrecht, D., Wiechert, L., Weih, D., and Weih, F. (2012). p100 Deficiency is insufficient for full activation of the alternative NF-κB pathway: TNF cooperates with p52-RelB in target gene transcription. PLoS ONE *7*, e42741.

Luftig, M.A., Cahir-McFarland, E., Mosialos, G., and Kieff, E. (2001). Effects of the NIK aly mutation on NF-kappaB activation by the Epstein-Barr virus latent infection membrane protein, lymphotoxin beta receptor, and CD40. J. Biol. Chem. *276*, 14602–14606.

Meyer, H., Bug, M., and Bremer, S. (2012). Emerging functions of the VCP/p97 AAA-ATPase in the ubiquitin system. Nat. Cell Biol. *14*, 117–123.

Mordmüller, B., Krappmann, D., Esen, M., Wegener, E., and Scheidereit, C. (2003). Lymphotoxin and lipopolysaccharide induce NF-kappaB-p52 generation by a co-translational mechanism. EMBO Rep. *4*, 82–87.

Orian, A., Gonen, H., Bercovich, B., Fajerman, I., Eytan, E., Israël, A., Mercurio, F., Iwai, K., Schwartz, A.L., and Ciechanover, A. (2000). SCF(beta)(-TrCP) ubiquitin ligase-mediated processing of NF-kappaB p105 requires phosphorylation of its C-terminus by IkappaB kinase. EMBO J. *19*, 2580–2591.

Picotti, P., Bodenmiller, B., Mueller, L.N., Domon, B., and Aebersold, R. (2009). Full dynamic range proteome analysis of S. cerevisiae by targeted proteomics. Cell *138*, 795–806.

Qing, G., Qu, Z., and Xiao, G. (2005). Stabilization of basally translated NF-kappaB-inducing kinase (NIK) protein functions as a molecular switch of processing of NF-kappaB2 p100. J. Biol. Chem. *280*, 40578–40582.

Razani, B., Reichardt, A.D., and Cheng, G. (2011). Non-canonical NF-κB signaling activation and regulation: principles and perspectives. Immunol. Rev. *244*, 44–54.

Remouchamps, C., Boutaffala, L., Ganeff, C., and Dejardin, E. (2011). Biology and signal transduction pathways of the Lymphotoxin-αβ/LTβR system. Cytokine Growth Factor Rev. *22*, 301–310.

Savinova, O.V., Hoffmann, A., and Ghosh, G. (2009). The Nfkb1 and Nfkb2 proteins p105 and p100 function as the core of high-molecular-weight heterogeneous complexes. Mol. Cell *34*, 591–602.

Scheidereit, C. (2006). IkappaB kinase complexes: gateways to NF-kappaB activation and transcription. Oncogene *25*, 6685–6705.

Senftleben, U., Cao, Y., Xiao, G., Greten, F.R., Krähn, G., Bonizzi, G., Chen, Y., Hu, Y., Fong, A., Sun, S.C., and Karin, M. (2001). Activation by IKKalpha of a second, evolutionary conserved, NF-kappa B signaling pathway. Science *293*, 1495–1499.

Shih, V.F., Davis-Turak, J., Macal, M., Huang, J.Q., Ponomarenko, J., Kearns, J.D., Yu, T., Fagerlund, R., Asagiri, M., Zuniga, E.I., and Hoffmann, A. (2012). Control of RelB during dendritic cell activation integrates canonical and noncanonical NF-κB pathways. Nat. Immunol. *13*, 1162–1170.

Shinkura, R., Kitada, K., Matsuda, F., Tashiro, K., Ikuta, K., Suzuki, M., Kogishi, K., Serikawa, T., and Honjo, T. (1999). Alymphoplasia is caused by a point mutation in the mouse gene encoding Nf-kappa b-inducing kinase. Nat. Genet. *22*, 74–77.

Sriskantharajah, S., Belich, M.P., Papoutsopoulou, S., Janzen, J., Tybulewicz, V., Seddon, B., and Ley, S.C. (2009). Proteolysis of NF-kappaB1 p105 is essential for T cell antigen receptor-induced proliferation. Nat. Immunol. *10*, 38–47.

Stilmann, M., Hinz, M., Arslan, S.C., Zimmer, A., Schreiber, V., and Scheidereit, C. (2009). A nuclear poly(ADP-ribose)-dependent signalosome confers DNA damage-induced IkappaB kinase activation. Mol. Cell *36*, 365–378.

Sun, S.C. (2012). The noncanonical NF-κB pathway. Immunol. Rev. *246*, 125–140.

Vallabhapurapu, S., and Karin, M. (2009). Regulation and function of NF-kappaB transcription factors in the immune system. Annu. Rev. Immunol. *27*, 693–733.

Wolf-Yadlin, A., Hautaniemi, S., Lauffenburger, D.A., and White, F.M. (2007). Multiple reaction monitoring for robust quantitative proteomic analysis of cellular signaling networks. Proc. Natl. Acad. Sci. USA *104*, 5860–5865.

Xiao, G., Harhaj, E.W., and Sun, S.C. (2001). NF-kappaB-inducing kinase regulates the processing of NF-kappaB2 p100. Mol. Cell *7*, 401–409.

Yamanaka, K., Sasagawa, Y., and Ogura, T. (2012). Recent advances in p97/VCP/Cdc48 cellular functions. Biochim. Biophys. Acta *1823*, 130–137.

Yilmaz, Z.B., Weih, D.S., Sivakumar, V., and Weih, F. (2003). RelB is required for Peyer's patch development: differential regulation of p52-RelB by lymphotoxin and TNF. EMBO J. *22*, 121–130.

Zhang, Z., Lv, X., Yin, W.C., Zhang, X., Feng, J., Wu, W., Hui, C.C., Zhang, L., and Zhao, Y. (2013). Ter94 ATPase complex targets k11-linked ubiquitinated ci to proteasomes for partial degradation. Dev. Cell *25*, 636–644.